

SANDIA REPORT

SAND2012-9348

Unlimited Release

Printed October, 2012

Design and Characterization of a Sodium Iodide (NaI) Array for Coincidence Measurements

Gregory G. Thoreson, Dean J. Mitchell, Charles A. Brusseau,
Lee T. Harding, and Lester H. Arakaki

Prepared by
Sandia National Laboratories
Albuquerque, New Mexico 87185 and Livermore, California 94550

Sandia National Laboratories is a multi-program laboratory managed and operated by Sandia Corporation, a wholly owned subsidiary of Lockheed Martin Corporation, for the U.S. Department of Energy's National Nuclear Security Administration under contract DE-AC04-94AL85000.

Approved for public release; further dissemination unlimited.



Sandia National Laboratories

Issued by Sandia National Laboratories, operated for the United States Department of Energy by Sandia Corporation.

NOTICE: This report was prepared as an account of work sponsored by an agency of the United States Government. Neither the United States Government, nor any agency thereof, nor any of their employees, nor any of their contractors, subcontractors, or their employees, make any warranty, express or implied, or assume any legal liability or responsibility for the accuracy, completeness, or usefulness of any information, apparatus, product, or process disclosed, or represent that its use would not infringe privately owned rights. Reference herein to any specific commercial product, process, or service by trade name, trademark, manufacturer, or otherwise, does not necessarily constitute or imply its endorsement, recommendation, or favoring by the United States Government, any agency thereof, or any of their contractors or subcontractors. The views and opinions expressed herein do not necessarily state or reflect those of the United States Government, any agency thereof, or any of their contractors.

Printed in the United States of America. This report has been reproduced directly from the best available copy.

Available to DOE and DOE contractors from
U.S. Department of Energy
Office of Scientific and Technical Information
P.O. Box 62
Oak Ridge, TN 37831

Telephone: (865) 576-8401
Facsimile: (865) 576-5728
E-Mail: reports@adonis.osti.gov
Online ordering: <http://www.osti.gov/bridge>

Available to the public from
U.S. Department of Commerce
National Technical Information Service
5285 Port Royal Rd.
Springfield, VA 22161

Telephone: (800) 553-6847
Facsimile: (703) 605-6900
E-Mail: orders@ntis.fedworld.gov
Online order: <http://www.ntis.gov/help/ordermethods.asp?loc=7-4-0#online>



Design and Characterization of a Sodium Iodide (NaI) Array for Coincidence Measurements

Gregory G. Thoreson, Dean J. Mitchell, Charles A. Brusseau,
Lee T. Harding, and Lester H. Arakaki

Contraband Detection Department 6633

MS-0782

Sandia National Laboratories

P.O. Box 5800

Albuquerque, New Mexico 87185

Abstract

An array of sodium iodide detectors (NaI) was constructed to record time-correlated gamma ray measurements. The NaI Array consists of twelve 2×4×16-inch detectors. When the array is placed close to an inspected object, this arrangement provides high efficiency for gamma ray detection, particularly for high-energy gamma rays. Data are collected in time-tagged, list-mode format, which is suitable for the application of a variety of coincidence analysis methods.

Automated energy calibration of each detector is accomplished by utilizing gamma radiation from thoriated welding rods that are embedded in the system. The energy resolution of spectra that are produced by the NaI array is 7.3% at 662 keV. The data are processed to sum gamma-ray energies for simultaneous detections in adjacent detectors, which are dominated by the escape of scattered photons from one detector and subsequent absorption in an adjacent detector. When data are processed in this way, the photopeak efficiency exceeds 20% over the range 400 keV to 10 MeV; the total efficiency, which includes the Compton continuum and single and double escape peaks, exceeds 70% over this energy range. Utilization of time correlations enables isolation of spectral features that are associated with the same decay cascade or fission event. Characterization of the response of the NaI Array to both gamma rays and neutrons with the Gamma Detector Response and Analysis Software (GADRAS) enables accurate computation for virtually any radiation sources.

Acknowledgments

The authors would like to acknowledge the support and conception of this detector design from David Beach in Department of Energy Office of Nuclear Nonproliferation.

We also appreciate assistance provided by Andrew Glenn and Ron Wurtz of LLNL, who provided the data acquisition electronics and recommendations for operational settings.

Contents

1. Introduction.....	7
1.1. Design Concept.....	7
2. Hardware.....	9
2.1 Detector.....	9
2.2 Photomultiplier Tube Base	9
2.3 Data Acquisition	10
2.4 Integration.....	11
3. Setup and Testing.....	13
4. Detector Calibration and Summing	15
4.1 Energy Calibration.....	15
4.2 Spectrum Summing.....	18
4.3 Parsing Software	22
5. Detector Characterization.....	23
5.2 Gamma-Ray Response.....	23
5.3 Neutron Response	25
5.4 Dead Time Characterization	26
6. Conclusions.....	31
References.....	33
Distribution.....	34

Figures

Figure 1. Section drawing of NaI Array	8
Figure 2. Single NaI detector with PMT.....	9
Figure 3. Photomultiplier tube base.....	10
Figure 4. Data acquisition hardware	10
Figure 5. Cross-sectional drawing of detectors in housing.....	11
Figure 6. Consolidated cable connections in rear of detector housing	12
Figure 7. View of front of detector housing mounted on cart	13
Figure 8. Example un-calibrated background spectrum	14
Figure 9. Background spectrum for a single detector with a 50-MeV energy range.....	14
Figure 10. Gain and offset as a function of time.....	17
Figure 11. Adjacent event summing illustration.....	18
Figure 12. Simple (green) versus adjacent (blue) summing for background.....	19
Figure 13. Simple (green) versus adjacent (blue) summing for ^{252}Cf in PVC.....	20
Figure 14. Adjacent sum spectrum (green) versus the coincidence-only spectrum (blue) derived by processing the same list-mode data for a background measurement.....	21
Figure 15. Adjacent sum spectrum (green) versus the coincidence-only spectrum (blue) derived from a measurement of ^{252}Cf inside an 8-cm-thick PE sphere	22
Figure 16. Comparison of measured spectra (black error bars) with computed spectra (red) for the weak gamma-ray sources	24
Figure 17. Intrinsic photopeak efficiency curves for the NaI Array versus a single detector element.....	25

Figure 18. Comparison of measured (black) to calculation with neutron response (red) and calculation with no neutron response (blue) for a single NaI detector from a Cf-252 source bare (left panel) and surrounded by 8 cm of PE (right panel).....	26
Figure 19. Dead time as a function of count rate for detector 6	27
Figure 20. Effect of LLD on background spectrum.....	28
Figure 21. Effect of LLD on ¹³⁷ Cs source.....	29

Tables

Table 1. Detector PMT base Voltage Settings.....	13
Table 2. Base Offsets and Full-Scale Energies for Each Detector	15
Table 3. Gamma Energies Used in Deviation Pair Data.....	16
Table 4. Calibration Source Information	23
Table 5. Effect of LLD on Total Count Rates for the NaI Array.....	29

1. Introduction

This paper describes the development and characterization of a “NaI Array”, which consists of twelve, closely spaced 2×4×16-inch NaI detectors. Sodium iodide (NaI) is an inexpensive scintillating material that exhibits high light yield per unit energy (38,000 photons per MeV for NaI doped with thallium). Typical photopeak energy resolution for these crystals is 6.5-8% full-width-at-half-maximum (FWHM) at 662 keV. These crystals exhibit a 230 nanosecond decay constant for the primary scintillation pulse, which is orders of magnitude longer than organic scintillators¹. However, NaI detectors have much greater photopeak efficiencies, which make them attractive for applications that utilize spectroscopic information, particularly when timing resolution on the order of 100 nanoseconds is acceptable.

Timing information from the pulses in discrete detector elements allows the array to operate as a multiplicity counter. For example, two gamma rays are emitted almost simultaneously when ⁶⁰Co decays, but they can be resolved as correlated discrete gamma rays if they are absorbed in separate crystals within the array. In a similar way, the NaI Array can resolve multiple prompt fission gamma rays from a single fission event and fission chains. Data recorded by the NaI Array will also be used to investigate correlations between the prompt fission gamma rays and correlated but delayed events, such as detection of neutron capture gamma rays and events that are recorded by neutron multiplicity counters.

1.1. Design Concept

Twelve detectors can be arranged in a variety of configurations. It is a balance between the intrinsic efficiency of the system and the solid angle subtended. As a compromise, the detectors are placed such that they are 4 inches deep, 2 inches in height, and 16 inches in width. This arrangement also reduces the count rate for individual detector elements relative to rates that would be observed if the detectors were rotated 90° (where the detectors would be 2 inches deep, 4 inches high, and 16 inches wide), which enables operating in higher radiation fields without experiencing excessive random pileup. The ends of the detectors are alternated from one edge of the detector stack to the other, as in Figure 1, in order to arrange the active material as close together as possible. The backs of the detectors are shielded with 3/8-inch of lead to reduce background radiation. In anticipation of high dead-time from strong sources, the front plane is shielded with 1/8-inch of lead, which reduces the count rate for low-energy gamma radiation while having little impact on gamma rays exceeding 1 MeV. Sheets of 0.060-inch-thick tin are interposed between the lead and the detector to attenuate lead x-rays.

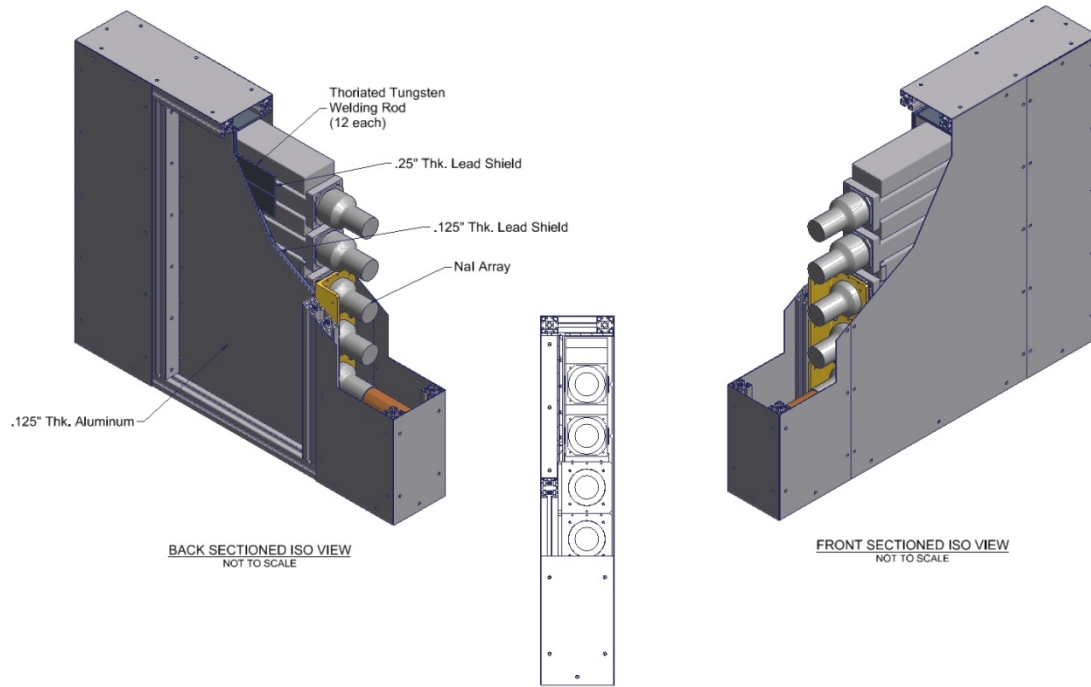


Figure 1. Section drawing of NaI Array

2. Hardware

2.1 Detector

The NaI detectors are 2×4×16-inch rectangular crystals manufactured by Saint-Gobain. The photomultiplier tube (PMT) is 3.5 inches in diameter. A picture of a detector with PMT is shown in Figure 2. The NaI crystals are enclosed within aluminum housings.



Figure 2. Single NaI detector with PMT

2.2 Photomultiplier Tube Base

Two views of the Ortec DIM-296 tube base are shown in Figure 3. The tube base has the standard 14-pin socket which attaches directly to the end of the PMT shown in Figure 2. Signals are passed directly from the anode on the PMT base to the digitizer, so the internal preamplifier and signal lines on the cable are not used. Custom connectors which only supply power (12 VDC, 240 mW) to the PMT base were constructed, and coaxial cables from the anode outputs are run directly to digitizer boards. High voltages for the photomultiplier dynodes are generated within the DIM-296, which avoids the need to provide a high voltage from an external high-voltage power supply.



Figure 3. Photomultiplier tube base

2.3 Data Acquisition

BNC-to-LEMO converters are used to interface the BNC anode outputs from the tube bases to the digitizer boards, which use LEMO connectors. A set of twelve coaxial cables with LEMO connectors run directly from the BNC-to-LEMO converters to the inputs on Struck SIS3302 Digitizer boards. The digitizers are inserted into a Wiener VME195 crate along with a Struck SIS3150 USB interface board as shown in Figure 4 in the left panel. The right panel shows the system operating with two digitizers. Because the NaI array has twelve detectors two digitizer boards are required, as each digitizer board can only accommodate eight detectors. A USB cable from the USB Control Board is connected to a data acquisition computer. Additional digitizer boards can be inserted into the VME195 crate to enable operation of the NaI Array in conjunction with other detectors, such as neutron counters. A Struck SIS3820 Clock Distributor board is used to synchronize the digitizers to a common clock.

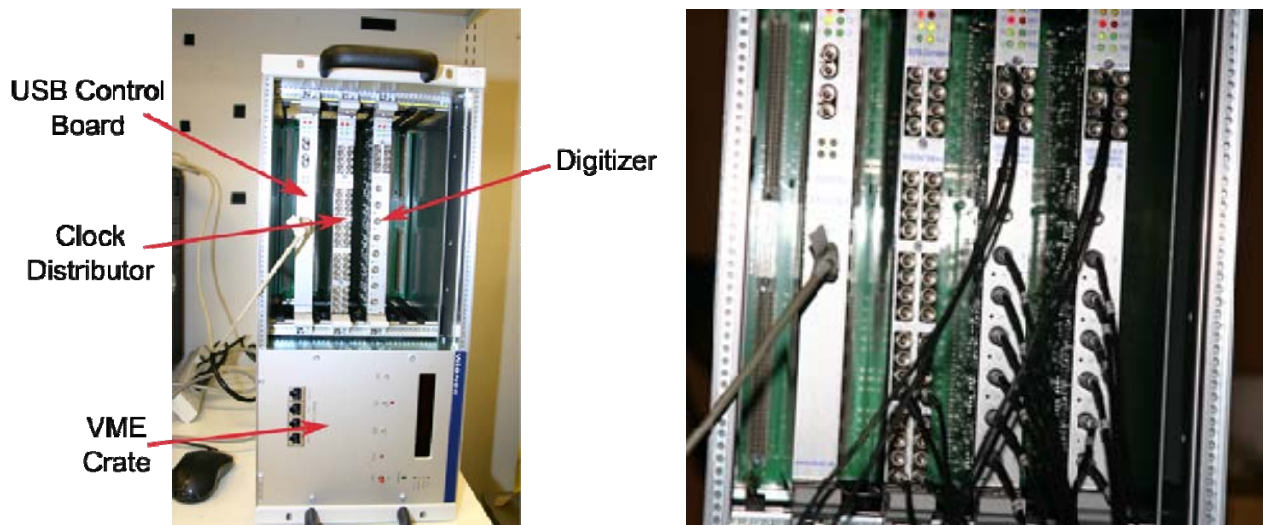


Figure 4. Data acquisition hardware

Struck supplies USB drivers that are compatible with the data acquisition computer, which runs under a Linux operating system (Ubuntu 10.04 64 bit). Software developed by Lawrence Livermore National Laboratory is used to control the digitizer settings.

2.4 Integration

The twelve detectors are individually mounted to brackets that are attached to an extruded aluminum frame. The detectors, PMT bases, power cables, and signal cables are contained inside an aluminum enclosure. Twelve thoriated welding rods are embedded in troughs in a lead shield on the back side of the detectors (see Figure 5). The welding rods are recessed between lead sheets to reduce the probability that emitted gamma-rays will strike a detector other than the one closest to the welding rod. The rods are centered and run parallel to the long dimensions of the detectors. Figure 5 shows a cross section through the NaI Array.

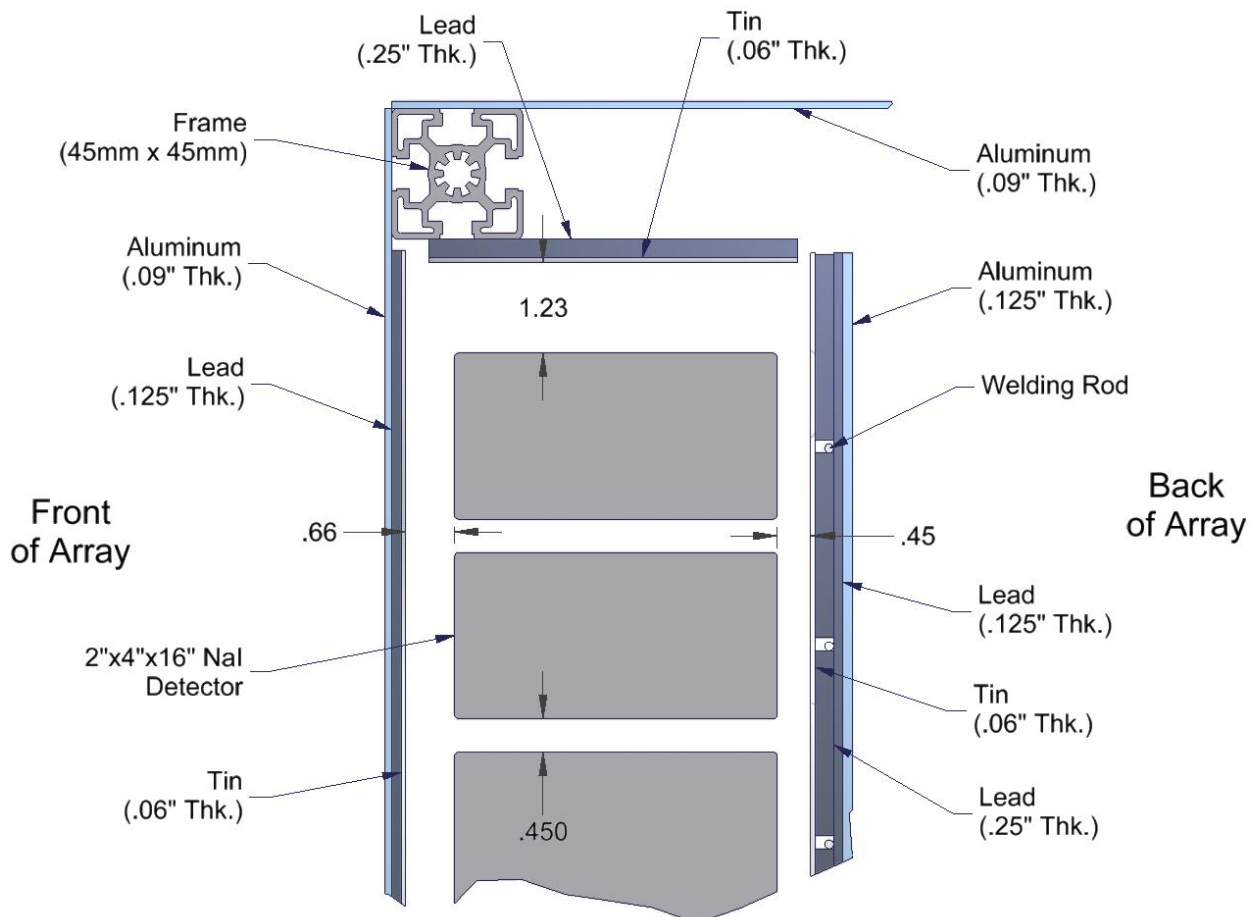


Figure 5. Cross-sectional drawing of detectors in housing

The power cables from the twelve detectors are consolidated to a single plug on the back side of the detector housing as shown in Figure 6. Also on the back left and back right sides of the

housing there are six signal cable plugs. The detectors are numbered using the convention that the first detector is on the bottom of the array and the twelfth detector is at the top. Thus, because of their staggered arrangement, the PMT bases and signal cable plugs for odd-numbered detectors reside on one side of the array (left side if facing the front of the array), and even-numbered detectors are located on the opposite side.

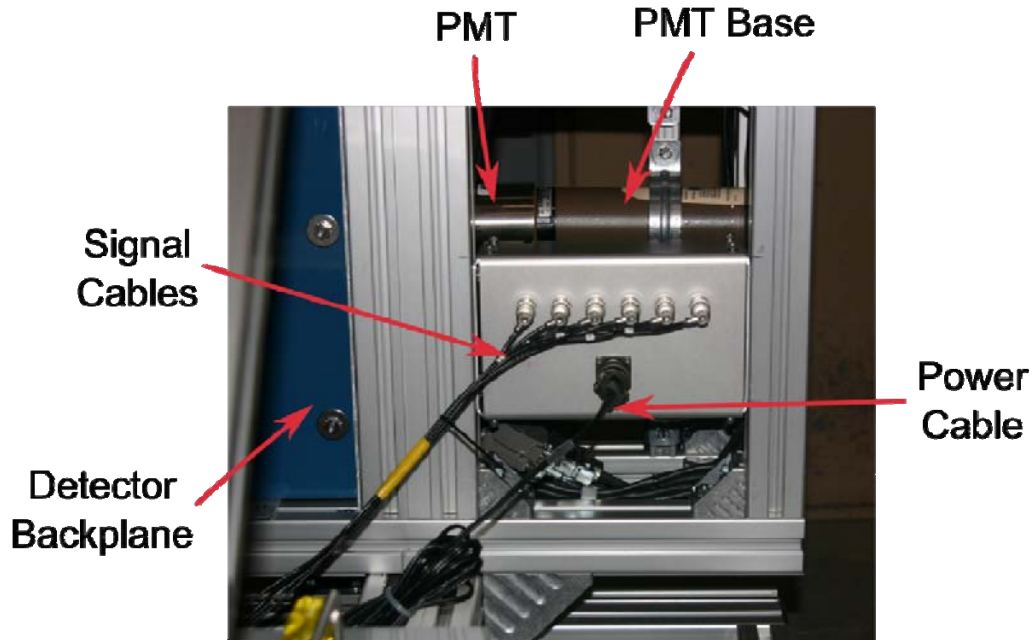


Figure 6. Consolidated cable connections in rear of detector housing

The detector housing is mounted on a cart constructed of extruded aluminum pieces as shown in Figure 7. The data acquisition equipment and computer are not attached to the cart. Because the NaI Array with shielding and housing weighs approximately 600 pounds, iron brick counterweights are added to the rear of the cart for stability. With the counterweight, the entire system weighs approximately 1270 pounds.

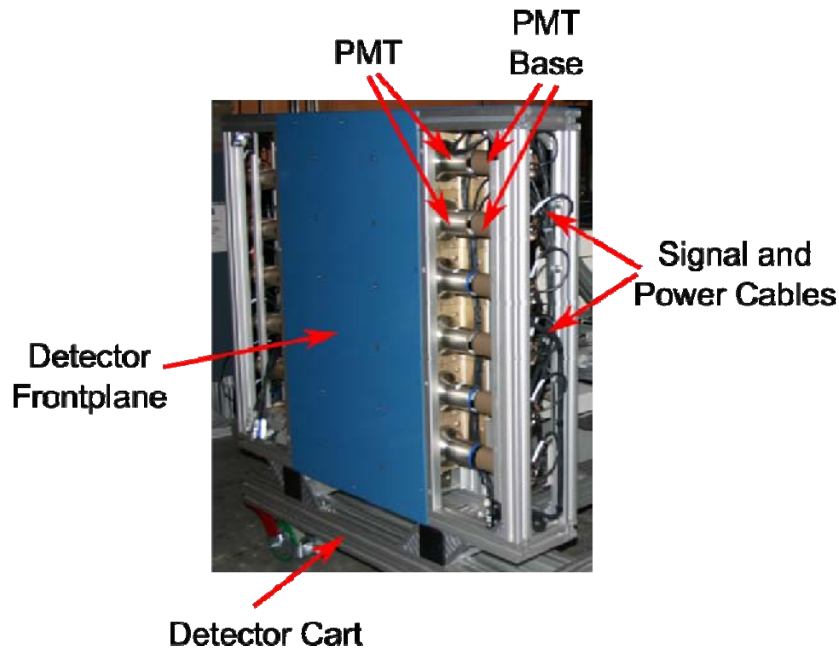


Figure 7. View of front of detector housing mounted on cart

3. Setup and Testing

With power applied to the PMT bases, the voltages on each were adjusted such that the gain was approximately equal on each detector, as measured by the position of the 2614 keV photopeak in the spectra. Gain and offset drift over time, so energy calibration is performed independently for each detector during data collections. Ideally, the voltage would be set as high as possible on each PMT base to maximize the resolution at low energies. Detector number 9 exhibited the lowest full-scale energy range at the maximum PMT voltage of 1100 V. Therefore, the voltages on the other detectors were adjusted to match the range achieved by detector 9. The resulting voltages ranged from 900 V to 1100 V, as shown in Table 1. Spectra were collected using different integrating times on the digitizer. A 1.0 μ s integration time for each pulse appeared to give good resolution while not adding unnecessary dead time.

Table 1. Detector PMT base Voltage Settings

Detector	Voltage (V)	Detector	Voltage (V)
1	1070	7	968
2	1087	8	1003
3	985	9	1101
4	1063	10	978
5	1005	11	943
6	965	12	951

The list-mode data is binned into 32,768 channels. An example background spectrum for the first three detectors is shown in Figure 8. A few common photopeaks for the blue spectrum are labeled. Note that all background measurements collected with this array record the signal from the embedded thoriated welding rods.

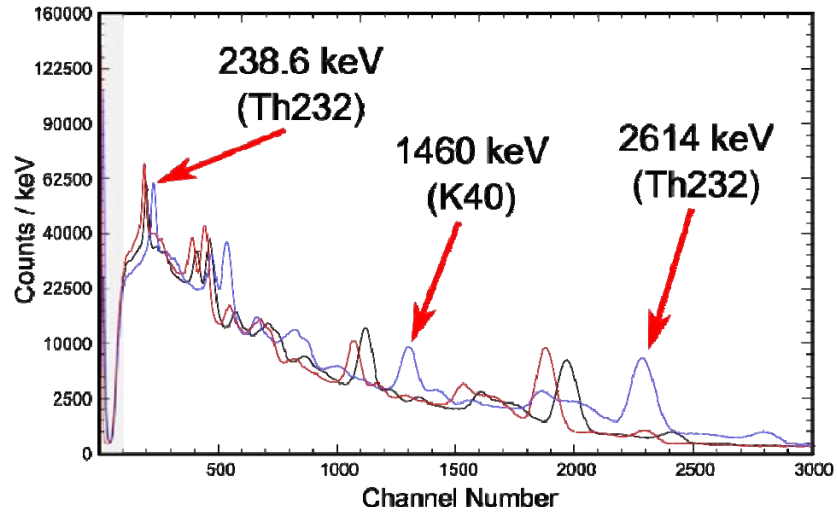


Figure 8. Example un-calibrated background spectrum

Figure 9 shows a background spectrum for a single detector when the full-scale energy range was set to approximately 50 MeV. The broad peak at channel 17,000 is produced by muons, which deposit approximately 27 MeV as they transit through a 2-inch-thick NaI crystal.

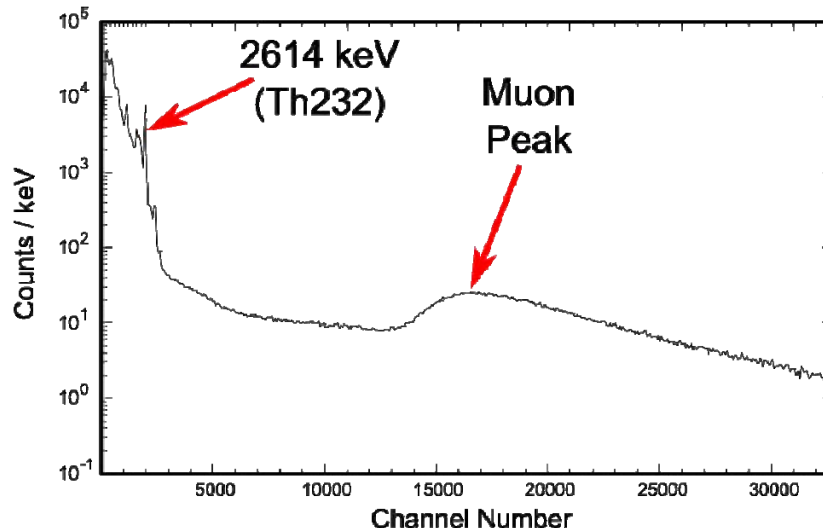


Figure 9. Background spectrum for a single detector with a 50-MeV energy range

4. Detector Calibration and Summing

4.1 Energy Calibration

Individual energy calibration parameters must be determined for each detector and adjusted periodically to accommodate gain and offset drift. However, previous work² has shown that the deviations from linearity are a relatively invariant property of a specific NaI crystal/PMT combination, so deviations that are determined from characterization spectra can be applied to subsequent measurements.

The 239 keV and 2614 keV peaks derived from gamma rays emitted by ²³²Th in the welding rods are used to adjust offset and gain parameters. Table 2 summarizes offset and full-scale energy (gain multiplied by the number of channels) parameters that were determined for each detector using high-voltage adjustments specified in Table 1. Characterization spectra (see Section 5) were then inspected to determine deviations in photopeak centroids relative to linear energy calibrations based on the gain and offset parameters. Table 3 lists the energies at which deviations were determined. A cubic spline fit of the deviations is used to define unique energy group structures for each detector.

Table 2. Base Offsets and Full-Scale Energies for Each Detector

Detector #	Offset (keV)	Full-Scale Energy (keV)
1	-23	21900
2	-21	18800
3	-24	22900
4	-23	19500
5	-25	22000
6	-24	22000
7	-27	20400
8	-27	20900
9	-24	20900
10	-25	20000
11	-28	21000
12	-26	20600

Table 3. Gamma Energies Used in Deviation Pair Data

Energy (keV)	Source
*239	²³² Th (welding rod)
356	¹³³ Ba
583	²³² Th (welding rod)
662	¹³⁷ Cs
1173	⁶⁰ Co
1460	⁴⁰ K
*2614	²³² Th (welding rod)
6110	Neutron capture by chlorine
7413	Neutron capture by chlorine

*Deviations were defined to be zero at these energies.

Figure 10 shows the time dependence of evaluated gain and offset parameters for each detector during a 16-hour background measurement. The gain and offset are computed every fifteen minutes for each detector. Each is normalized to the first calculated value; thus, the plots illustrate the relative fractional change. The gains drift by up to 1% (or within 26 keV at the 2614 keV peak) over the sixteen hours of measurement. Ignoring minor variations in time, which are most likely due to the limitations in precisely identifying the centroids, the drift rates are approximately constant. The linear, monotonic nature allows a background measurement before and after each source measurement to determine the slope and intercept of the gain drift. It is interesting to note that slopes of the gain drift are positive for some detectors and negative for other detectors. The offset does not appear to change appreciably over time, but spurious changes on the order of 10% (or approximately 2 keV) are observed for some detectors. The stability of the offset terms will be monitored during future measurements to determine whether frequent offset adjustments are essential.

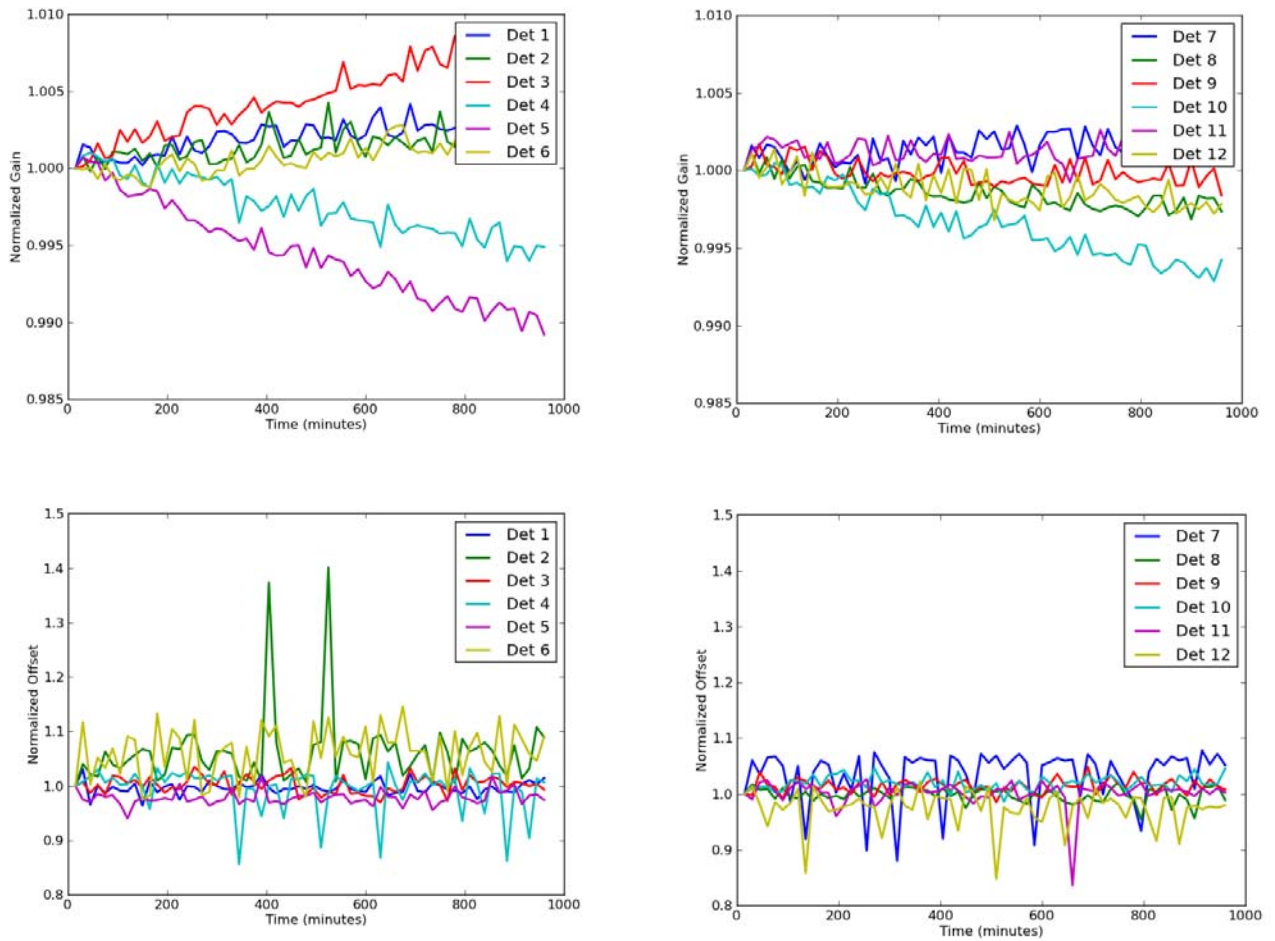


Figure 10. Gain and offset as a function of time

The following process is applied to convert pulse areas, which are recorded in the list-mode data, to energy units:

- The list-mode data are parsed and spectra are constructed for each detector during 15-minute intervals.
- Gain and offset parameters are determined for each detector so that peaks at 239 keV and 2614 keV correspond to the correct energies. Previous gain and offset parameters are applied without adjustment if poor fits are obtained for the calibration peaks or inspection of the data reveals that other radiation sources may interfere with determination of the peak centroids.
- Cubic-spline fits to the deviation pairs (deviation versus gamma-ray energy) are applied to generate unique energy-group structures for each detector.
- Individual pulses are converted to equivalent gamma-ray energies using the inferred energy-group structures.

4.2 Spectrum Summing

The signals from the detectors must be summed in order to synthesize a spectrum for the entire array. However, a simple addition of the signals ignores events in adjacent detectors that originate from a single source photon. These events are generally derived from Compton scattering out of one detector followed by absorption in the adjacent detector. This phenomenon could overwhelm correlations in the array.

The digitizer for this system is capable of resolving the onset of a pulse to within 50 nanoseconds. With this degree of resolution, events occurring simultaneously (within 50 nanoseconds) in adjacent detectors can be assumed to be either a scattering or pair-production event as illustrated in Figure 11. If a photon scatters in a detector and one adjacent detector registers a pulse simultaneously, then it is likely that it is a scattering and absorption event and the calibrated energy from both events can be summed. It is also possible that a scattered photon could pass through an intervening detector without depositing any energy before being absorbed in a non-adjacent detector, but to limit the interference on true coincidence measurements, this rarer event is not utilized in summing. Another event is the pair production in a crystal and absorption of one or both of the subsequent annihilation photons in one or two adjacent crystals. This is also assumed to correspond to a single event during which the photon energy is distributed among two or three detectors. The inference of original photon energy is improved by adding energies when simultaneous events are observed in adjacent detectors. The adjacent summing of detectors increases the photopeak efficiency of the system while also allowing the identification of true-coincidence events that occur in non-adjacent detectors. It is important to note that the adjacent summing is performed after energy calibration is performed and pulses are converted to energy units.

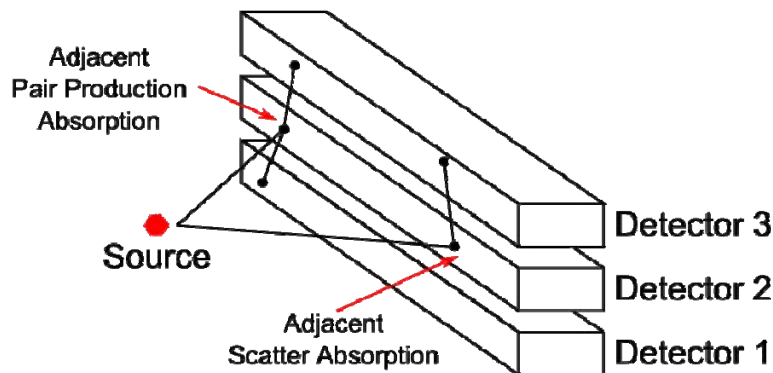


Figure 11. Adjacent event summing illustration

The effect of simple summing without accounting for simultaneous detections versus the adjacent detector summing approach described above is examined for representative measurements. Figure 12 compares a background spectrum for the NaI Array that was synthesized by simple summing with the spectrum that utilizes the adjacent summing approach. The count rates under the 1460 keV and 2614 keV peaks increased by 45% and 35%, respectively, using adjacent summing approach relative to simple summing. Furthermore, there is a pronounced decrease in the low-energy continuum because partial energy deposition is

reduced when adjacent summing is applied. Essentially, the array acts as its own Compton suppression system. Also noticeable in the adjacent summed spectrum is a significant increase in peaks higher than 2614 keV. These peaks are associated with true coincidence events derived from gamma rays at 2614, 583, 511, and 278 keV, which are emitted when the ^{208}Tl daughter decays. These coincidence events result from the close proximity of the welding rods to the detectors, and detections of coincident gamma rays are less probable for sources at a reasonable distance from the array.

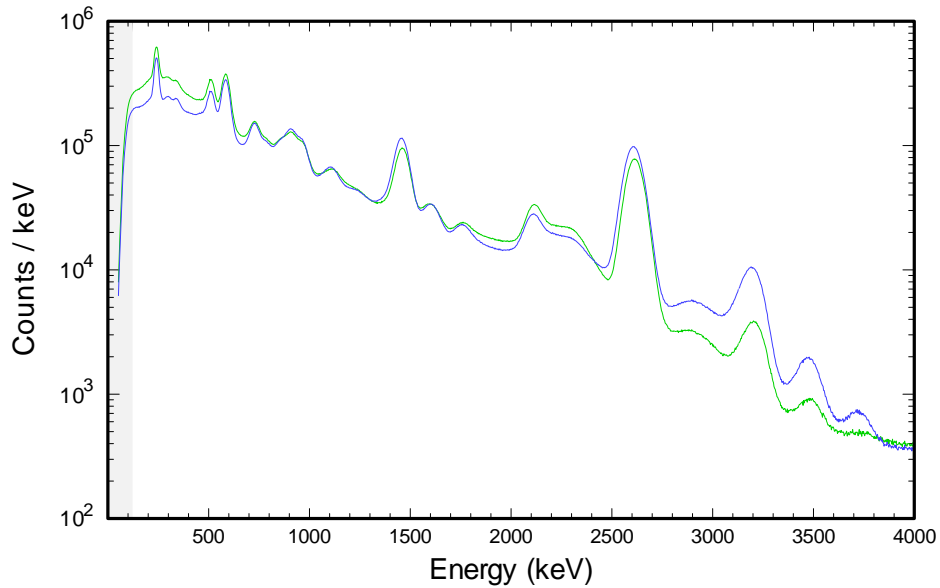


Figure 12. Simple (green) versus adjacent (blue) summing for background

One source measured with the NaI Array was ^{252}Cf within a polyvinyl chloride (PVC) shell, which emits a series of gamma rays extending to 8 MeV resulting from neutron capture by chlorine. Figure 13 compares background-subtracted spectra that were prepared by the simple sum and adjacent sum techniques. The trend that was observed for the background measurement is also replicated here, where the adjacent-sum spectrum exhibits greater photopeak efficiencies, and the low-energy continuum is also reduced.

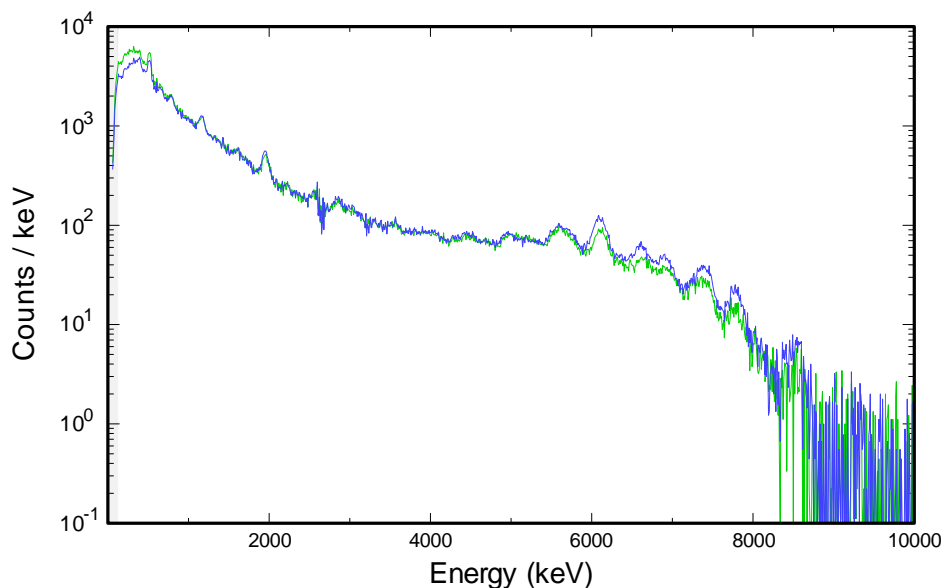


Figure 13. Simple (green) versus adjacent (blue) summing for ^{252}Cf in PVC

Another way to process the data is to only include events that are coincident (within 50 ns) in non-adjacent detectors, and sum the energy from events in adjacent detectors. Spectra prepared in this way are referred to as “coincident-only spectra”. This method isolates true coincidence events from the source while also increasing photopeak efficiency from adjacent summing. Figure 14 compares an adjacent sum background spectrum with a coincidence-only background spectrum that is synthesized by processing the same list-mode file. Noticeably absent from the coincidence-only spectrum is the 1460-keV peak from ^{40}K , which is not coincident with any other gamma rays. This implementation of the coincidence-only method accepts all events in non-adjacent detectors as coincidences regardless of the energy. The method could be expanded to establish energy windows for acceptance criteria.

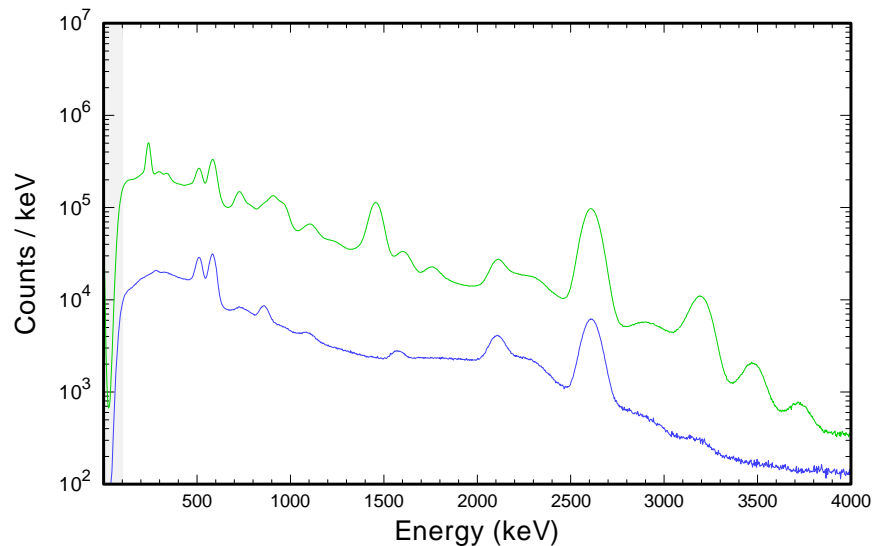


Figure 14. Adjacent sum spectrum (green) versus the coincidence-only spectrum (blue) derived by processing the same list-mode data for a background measurement

Figure 15 compares adjacent sum and coincidence-only spectra that were synthesized from a list-mode file that was collected while the NaI Array was exposed to a ^{252}Cf source inside an 8-cm-thick polyethylene (PE) shell. The appropriate background was stripped from each of the spectra shown in Figure 15 and Figure 14. Approximately 10 MeV of energy is emitted as prompt fission gammas per spontaneous fission of ^{252}Cf . This energy is shared, on average, among 7 to 10 gamma rays that are emitted per decay. These emissions give rise to a strong coincidence source, so fission gamma rays represent the principal component of the coincident-only spectrum. The peak in the low-energy region corresponds to the 511 keV gamma ray emitted by annihilation following pair production. This reaction is almost instantaneous relative to the 50-ns coincidence time window, so it appears in the coincidence-only spectrum along with the fission gamma rays. The 2223 keV peak is produced when neutrons are absorbed by hydrogen in the PE shell, and peaks in the 6-MeV region are produced when neutrons are absorbed by NaI (see Section 5.3). Both of the emissions are delayed with respect to the fission event since they occur following thermalization of the neutrons, on a time scale of about 10 μs . Consequently, peaks that are associated with absorption of low-energy neutrons are not observed in the coincident-only spectrum.

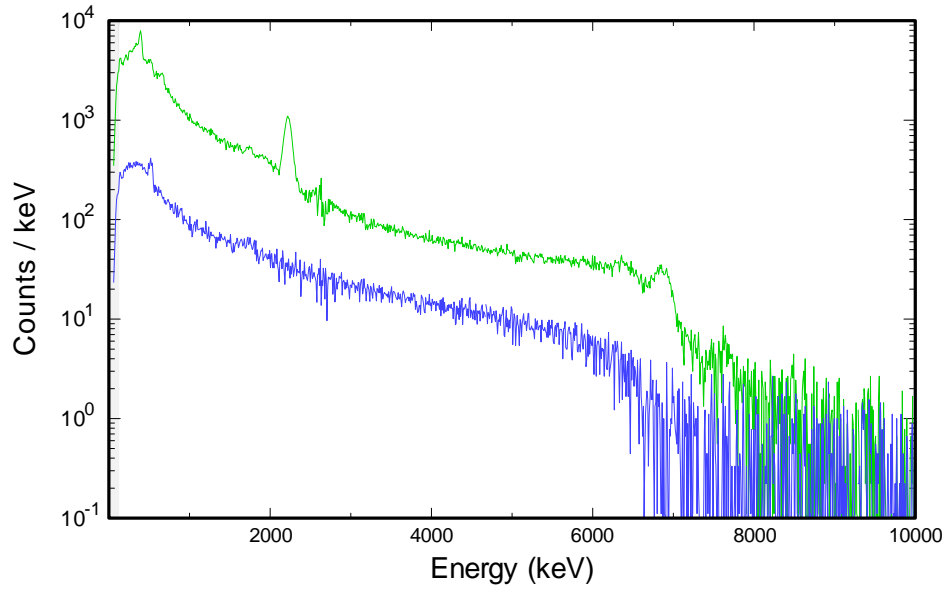


Figure 15. Adjacent sum spectrum (green) versus the coincidence-only spectrum (blue) derived from a measurement of ^{252}Cf inside an 8-cm-thick PE sphere

4.3 Parsing Software

The parsing, calibration, and analysis of the list-mode data is contained in the stand-alone program “naiparser”. It produces spectra for each detector individually before calibration and after calibration for each experiment, and produces three spectra for the entire array: a simple summation of all twelve signals, the adjacent summing accounting for adjacent coincident events, and the coincident only events.

5. Detector Characterization

A series of measurements were made with the following gamma-ray calibration sources: ^{133}Ba , ^{137}Cs , ^{60}Co , ^{232}U , and ^{252}Cf . The detector response of the detector to incident neutrons was also characterized by exposing the sensor to a ^{252}Cf source. Measurements were performed for the bare source, and the same source surrounded by spherical polyethylene (PE) moderators with the following thicknesses: 2 cm, 4 cm, and 8 cm. An additional measurement was recorded for the ^{252}Cf source inside an 8-cm-thick borated polyethylene moderator (BPE) in order to create a neutron-energy profile similar to ^{252}Cf inside the 8-cm-thick moderator except for the thermal region, which is greatly reduced by the large ^{10}B absorption cross-section. The ^{252}Cf source was also measured while it was surrounded by an 11.7-cm-thick shell of polyvinyl chloride (PVC). The objective of this measurement was to characterize the detector response at high energy (up to 8 MeV) by utilizing gamma rays that are emitted by chlorine following neutron capture reactions. Background spectra were recorded between source measurements to enable identification of energy-calibration peaks at 239 keV and 2614 keV, which were difficult to observe when some of the radiation sources were present.

All sources were suspended from an aluminum stand and centered on the front face of the array. Measurement distances and source activities were varied to characterize the performance over a range of count rates and coincident event rates. The source descriptions and measurement distances are summarized in Table 4.

Table 4. Calibration Source Information

Source Name	Serial Number	Calibration Activity (μCi)	Calibration Date	Distance(s)
^{137}Cs Strong	1351202	98.19	12/15/2008	100 cm, 25 cm
^{137}Cs Weak	1278693	19.24	02/15/2008	100 cm, 25 cm
^{60}Co Strong	1351203	100.41	12/15/2008	100 cm, 25 cm
^{60}Co Weak	1278691	10.12	02/15/2008	100 cm, 25 cm
^{133}Ba Strong	1351201	106.51	12/11/2008	100 cm
^{133}Ba Weak	1278692	19.54	02/15/2008	100 cm
^{232}U	NIST062322	10.00	08/01/2006	100 cm
^{252}Cf Strong	1672	228.81	03/01/2011	100 cm
^{252}Cf Weak	2641	215.00	06/09/2003	100 cm
^{137}Cs (ORNL)	5287	103.24	06/26/2012	various

5.2 Gamma-Ray Response

The NaI Array will normally be operated in the adjacent sum mode; thus, the detector response was characterized for spectra processed in this way. The GADRAS³ detector response function represents the detector array as if it were a single large detector except that the leakage of

scattered photons is increased (using the 54th parameter in the detector response settings) to match the response of the array empirically. The computed spectra for the weak gamma-ray sources are compared with measured, background-subtracted spectra in Figure 16. The chi-squared metric between the simulated detector signal and the measurement is 0.75, 0.82, 1.07, and 0.97 for ^{133}Ba , ^{137}Cs , ^{60}Co , and ^{232}U , respectively. This indicates reasonable agreement between the response function and the experimental data. The accuracy of the computed spectra for the NaI Array in adjacent sum mode is comparable to the accuracy of the computed response for individual detectors.

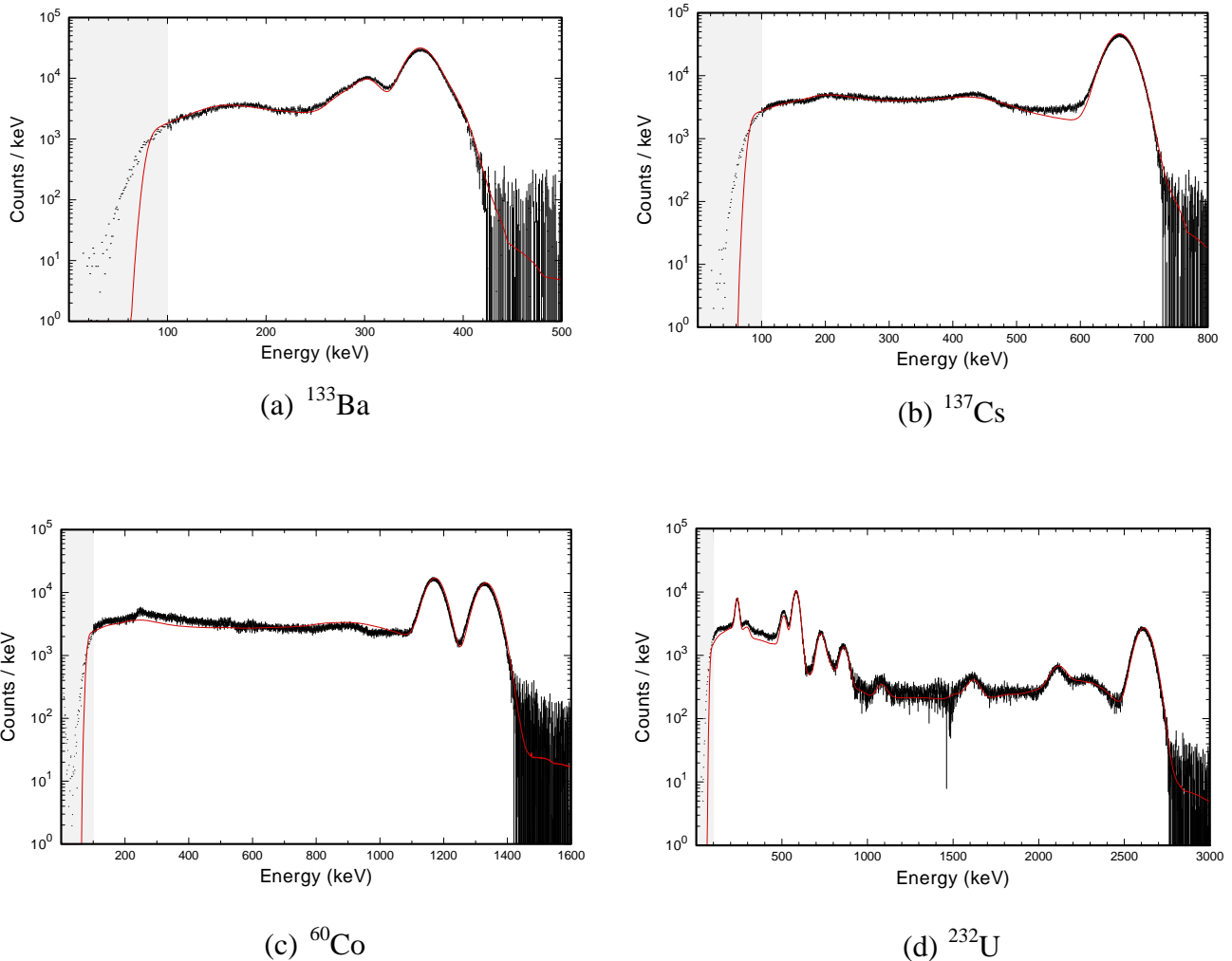


Figure 16. Comparison of measured spectra (black error bars) with computed spectra (red) for the weak gamma-ray sources

The detector characterization process generates a text file (Efficiency.csv) that lists the detector efficiency metrics as a function of the energy of the gamma-ray source. Figure 17 compares the

photopeak efficiency for the NaI Array with the photopeak efficiency for a single detector at the center of the array. The photopeak efficiency is expressed as the probability that a count is recorded in the photopeak per photon that strikes the detector surface directly. As expected, the difference is minimal at low energies (below about 400 keV) because the probability of a photon interacting with more than one crystal is small. The probability that a photon will be captured by an adjacent detector after scattering out of the primary detector increases for higher energy gamma rays, which improves the efficiency of the array relative to single crystals for moderate and high-energy gamma rays. Figure 17 also shows the total efficiency for the NaI Array, which includes the Compton continuum and single and double escape peaks. It is impressive to note that the total efficiency exceeds 70% for all energies exceeding 400 keV. The NaI Array is relatively insensitive to low-energy gamma rays because the incident photons are absorbed by the 1/8-inch-thick lead and the 0.060-inch-tin sheets of the front surface of the detector.

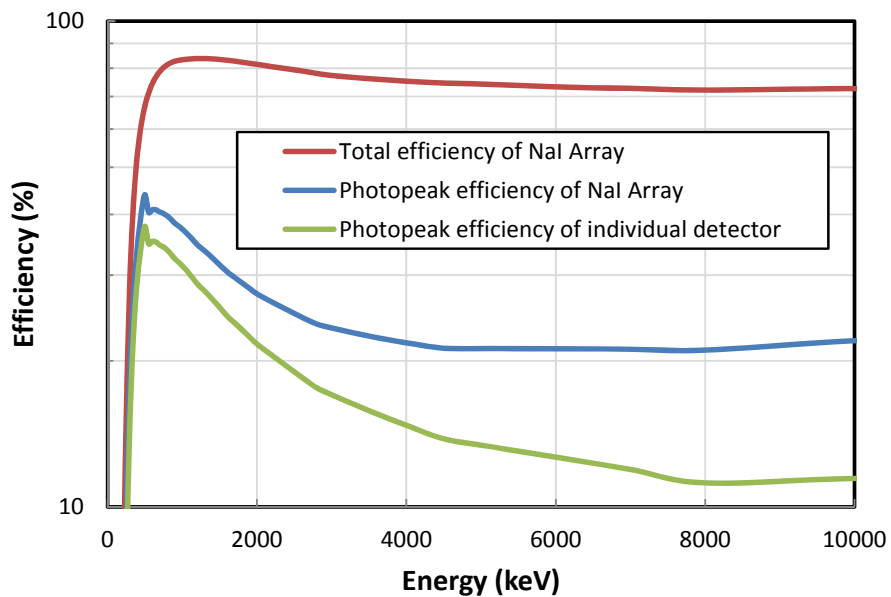


Figure 17. Intrinsic photopeak efficiency curves for the NaI Array versus a single detector element

5.3 Neutron Response

Gamma-ray detectors generally have low cross sections for neutron interactions, but they are not entirely insensitive to neutrons. One or more gamma rays with a total energy of about 10 MeV are emitted following neutron absorption in NaI. The GADRAS response function computes the neutron absorption rate based on published cross sections, and there are no adjustable parameters associated with this calculation other than the detector dimensions. Although the probability for generation of a gamma-ray continuum within the detector can be computed relatively easily, the energy distribution of the emitted gamma rays has not been characterized, and correlations among the energies of individual gamma rays add an additional complication. Therefore, the GADRAS response function applies an empirical template for the spectral shape when the response to incident neutrons is computed. The template is derived by interpolating

measurements based on the detector size. The NaI Array has a total volume of about 25 liters, which is much greater than the size of any NaI detector that had been characterized previously, so a new template was created for a detector with these dimensions. The template essentially represents the difference between a measurement of moderated ^{252}Cf and the computed spectrum that contains everything except the neutron response of the detector (i.e., fission gamma rays and neutron capture reactions outside of the detector are included). Although the neutron absorption rate varies with the neutron energy, the spectral shape of the detector response is insensitive to the neutron flux profile for NaI. Figure 18 compares measured spectra with calculations for bare ^{252}Cf and ^{252}Cf inside an 8-cm-thick PE sphere. The blue curves in these plots show calculations that do not include the neutron response of the NaI detectors. The measured data in these plots correspond to background subtracted, adjacent sum spectra.

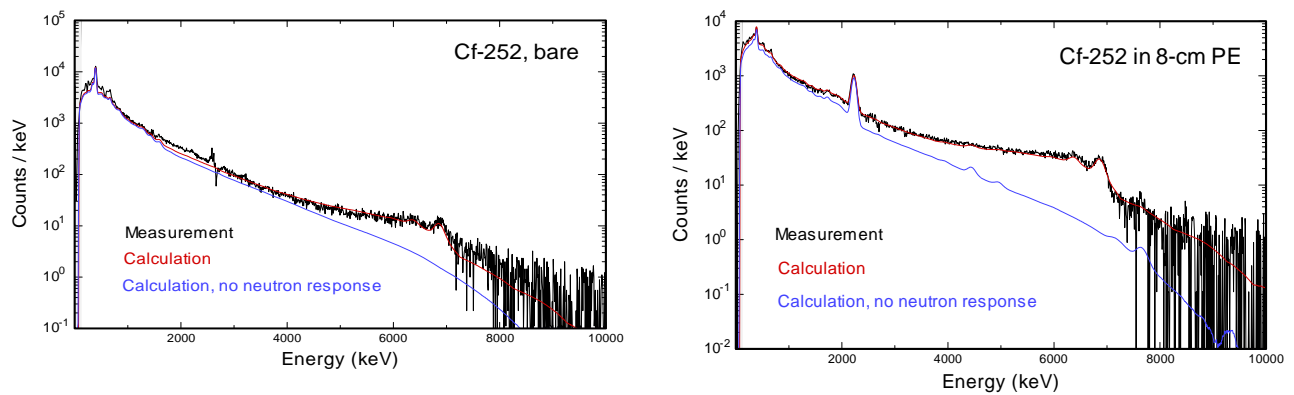


Figure 18. Comparison of measured (black) to calculation with neutron response (red) and calculation with no neutron response (blue) for a single NaI detector from a Cf-252 source bare (left panel) and surrounded by 8 cm of PE (right panel)

5.4 Dead Time Characterization

The Struck digitizers can operate in two modes: single and double buffering. With single buffering, the digitizer collects data in memory until the buffer is full, and then it transfers the data to the collection computer. The digitizer does not record new data while this transfer is in progress. With double buffering, the memory is segregated into two segments, and one half can acquire data while the other half transfers the data to the computer. The buffering dead time is essentially zero until the event or count rate exceeds the memory transfer rate. At this point, the dead time in single buffering mode is 50%, and in double buffering mode the digitizers will start overwriting memory blocks in the second buffer, causing data loss. A moving average of the count rate in each digitizer channel is maintained to account for the buffering dead time. Double buffering is preferable for operating the NaI Array, so this is the default mode that was selected for characterization measurements.

In addition to buffering dead time, there is dead time introduced by the integration time after each pulse. The Struck digitizers flag pulses that appear to have more than one pulse within the set integration time, but there is additional dead time caused by the electronics that is not well

understood. Thus, the dead time was characterized empirically by recording spectra while a 103 μCi ^{137}Cs source was placed at distances ranging from 5.7 cm to 305 cm from the front surface of the NaI Array. These measurements vary the count rate over a sufficient range to compute count rates, which are based on the dead time characterization, with experimental data for both a single detector and the entire array.

If the study is limited to the count rate under the 662 keV photopeak, the theoretical predictions are not dependent on the detector response function scattering models. The driving factor is the solid angle subtended by the detector, which is well understood and modeled in GADRAS. Furthermore, if only the relative change in count rate is considered, the theoretical absolute efficiency of the detector is irrelevant.

The count rates in the 662 keV photopeaks for measured spectra should be equal to count rates that are computed by GADRAS if the dead times are estimated correctly. Therefore, dead times can be determined from the ratios of the computed to measured peak areas. Figure 19 displays the observed relationship between percent dead time and the total count rate for detector #6, which is at the center of the NaI Array. For this experiment, the digitizers were operated in double buffering mode and no buffering dead time was apparent. The increase in dead time as a function of total count rate is approximately linear with a slope of 1.7 μs . This is consistent with the 1.4 μs integration gate used for each pulse and the additional dead time after the pulse from the electronics, which is known to be small but not well understood. This dead time and the buffering dead time estimates are incorporated into the parsing software, which outputs this into the spectral files.

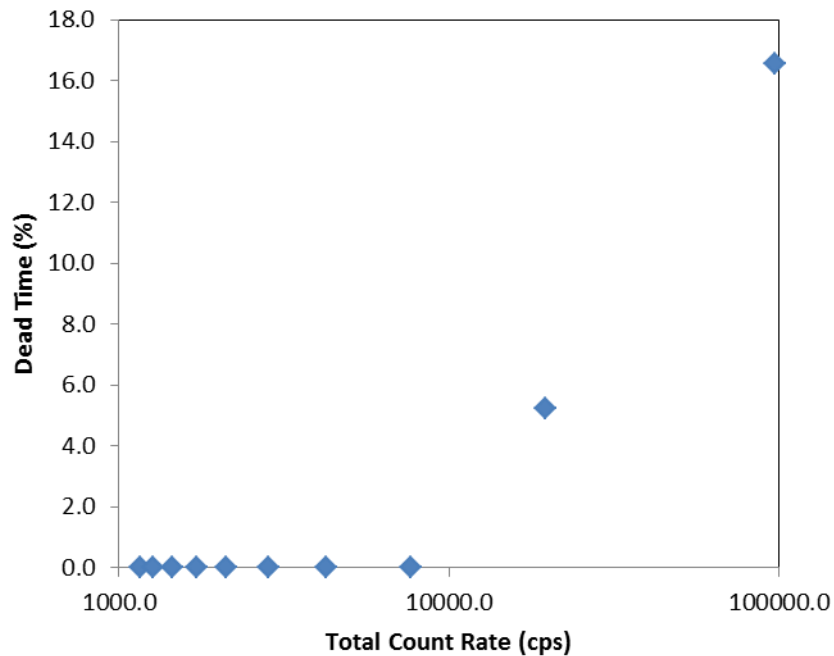


Figure 19. Dead time as a function of count rate for detector 6

This study shows that the total count rate for the sodium iodide array can in principal exceed 1 MHz with less than 20% dead time. However, it is not clear that the digitizers or data

collection computer can handle that data rate. As an option to reduce the count rate without any physical modification of the detection equipment, the lower-level discriminator (LLD) on the digitizers could be increased. The effect of varying the LLD was explored to determine whether any unanticipated consequences might be encountered. Most of the characterization measurements were collected with the LLD=14, which corresponds to an energy cutoff of 100 keV to 150 keV (depending on the detector). In our evaluation, the LLD was varied from 14 to 56 in increments of 14, which produced proportional changes in the energy cutoff. The effects on measured spectra are shown in Figure 20 and Figure 21. The total count rates for the system are tabulated in Table 5. It is important to note that in the background spectrum, the resolution or count rates for the photopeaks at higher energies are not affected by the LLD. Therefore, increasing the LLD is an attractive option for reducing the count rate from hot sources if the principal objective is utilization of high-energy gamma rays. Obviously, the effectiveness of increasing the LLD to reduce the overall count rate depends on the spectral shape. For the background spectrum, which is dominated by emission from the thoriated welding rods, most of the counts are in the lower energy range. Thus, increasing the LLD from 14 to 42 reduced the count rate by 55%, whereas the count rate only decreased by 40% for measurements of the ^{137}Cs source.

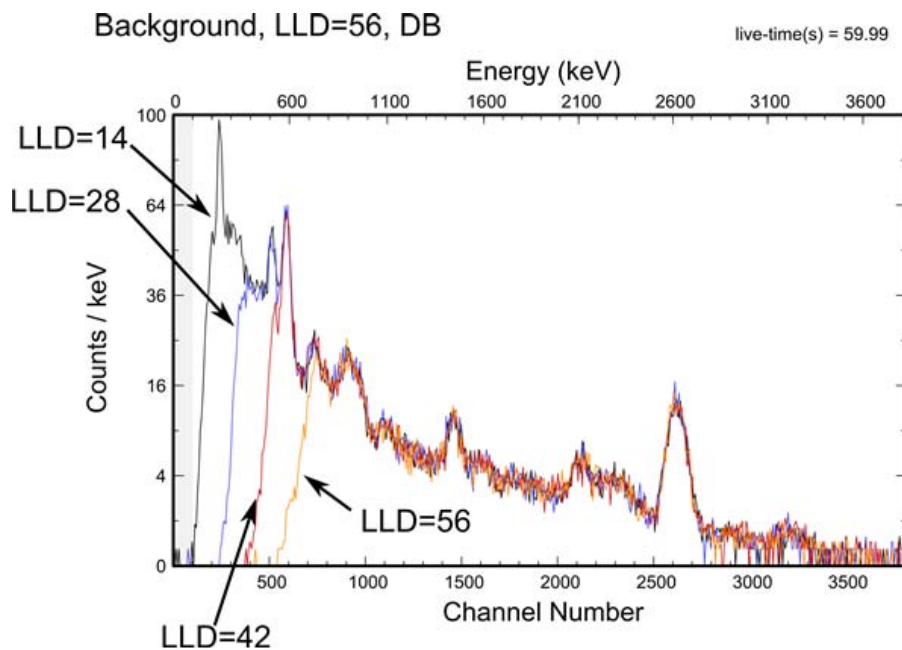


Figure 20. Effect of LLD on background spectrum

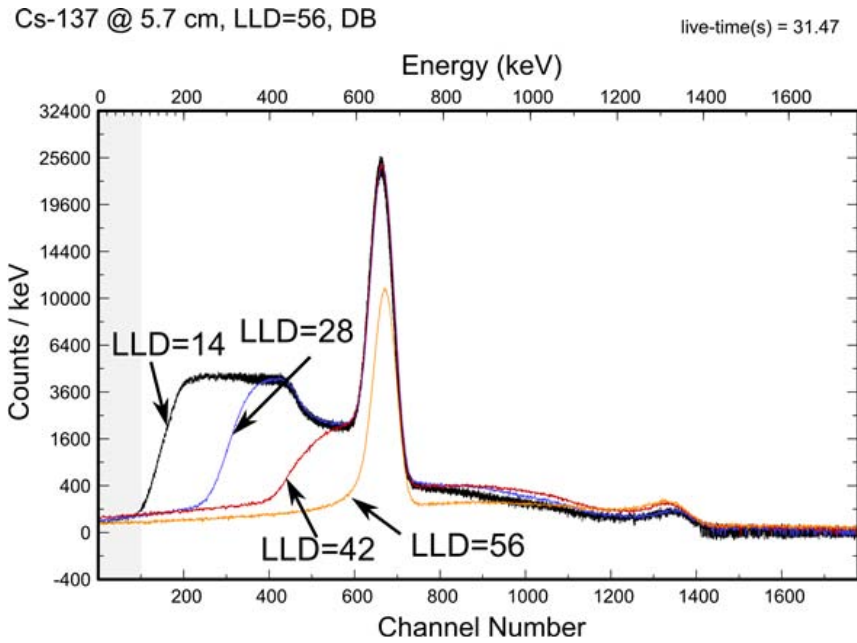


Figure 21. Effect of LLD on ^{137}Cs source

Table 5. Effect of LLD on Total Count Rates for the NaI Array

LLD	Background Count Rate	^{137}Cs Count Rate
14	656	97000
28	488	78000
42	363	58000
56	256	22000

Increasing the LLD from 14 will remove or distort photopeaks at 239 keV, which are used in conjunction with the 2614 keV peak to determine gain and offset parameters. Therefore, if a measurement requires the LLD to be increased, it is recommended that a 10 minute background with the LLD at 14 be taken before and after the experiment. Energy calibration parameters that are derived from the background spectra can then be interpolated for measurements that are recorded between the two background collections.

6. Conclusions

The constructed NaI Array performs as expected. The signal from each detector element is recorded in a time-tagged list-mode format. A calibration program post-processes the data to convert the digitized pulses into chronologically sorted energy deposition events. The calibrated data is again processed using a variety of algorithms to produce aggregate spectra for the array. Processing utilizes timing information to deduce scattering events between detector crystals and true coincident events from a source emitting multiple gamma rays, such as prompt fission gammas. Summing the energy deposited coincidentally in adjacent crystals increases the intrinsic efficiency of the array.

GADRAS was used to characterize a single NaI crystal and the entire array operating in adjacent-summation mode. The software was modified to allow for increased leakage of scattered photons relative to a single crystal of the same volume as the NaI Array. The array operates with a combined energy resolution of 7.3% at 662 keV, and the total efficiency exceeding 70% above 400 keV. The high efficiency of the array compared to a single detector element significantly increases the detection probability for high-energy gamma rays. GADRAS was modified to apply an empirical template to account for neutron absorption in the array.

The intrinsic efficiency and large solid angle subtended by the array make it suitable for gamma multiplicity measurements. However, it was discovered that coincidences from the embedded thoriated welding rods overwhelm the correlated signal associated with the presence of a weak fission source. Future modifications of this design will circumvent this problem by embedding an uncorrelated source (such as ^{40}K) or using removable welding rods. A ^6Li blanket may also be added to reduce neutron absorption by the NaI, which interferes with detection of high-energy neutrons emitted by inspected items.

The data acquisition equipment is capable of simultaneously collecting time-tagged events from neutron detectors. While not investigated in this report, neutron-gamma correlation measurements will be investigated. The energy resolution and efficiency above 3 MeV of the NaI Array make it useful for such correlations, especially considering that many of the gamma rays produced by neutron interactions have high energies. Measuring and studying these correlations is a topic of future work with the array.

References

1. Knoll, G.F., *Radiation Detection and Measurement*, p. 234, John Wiley & Sons, Inc., March 2000.
2. DNDO Document Number 600-ALIPT-000019 v 1.00, "Interface Control Document for DNDO Radiation Measurement Files.
3. Dean J. Mitchell, "Automated SNM Analysis for Gamma-Ray Spectra," SAND2008-6425C, Sandia National Laboratories, INMM/ESARDA, International Workshop on Gamma Spectrometry Analysis Codes for U and Pu Isotopics, Oak Ridge, Tennessee, November 2008.

Distribution

Hard Copies:

- 4 Lawrence Livermore National Laboratory
Attn: N. Dunipace (1)
P.O. Box 808, MS L-795
Livermore, CA 94551-0808

Electronic Copies:

- 1 David Beach, DOE/NNSA/NA-221 david.beach@nnsa.doe.gov (electronic copy)
U.S. Department of Energy
Routing: NA-221 1000
Independence Ave. SW
Washington DC 20585
- 1 Arden Dougan, DOE/NNSA/NA-221 arden.dougan@nnsa.doe.gov (electronic copy)
U.S. Department of Energy
Routing: NA-221
Independence Ave. SW
Washington DC 20585
- 1 Ron Wurtz, LLNL wurtz@llnl.gov (electronic copy)
Lawrence Livermore National Laboratory
P.O. Box 808, MS L-795
Livermore, CA 94551-0808
- 1 Les Nakae, LLNL nakae1@llnl.gov (electronic copy)
Lawrence Livermore National Laboratory
P.O. Box 808, MS L-795
Livermore, CA 94551-0808
- 1 Avneet Sood, LANL sooda@lanl.gov (electronic copy)
Los Alamos National Laboratory
P.O. Box 1663
Los Alamos, NM 87545
- 1 MS0899 Technical Library 9536 (electronic copy)

